Proceedings of IMECE'02
2002 ASME International Mechanical Engineering Congress & Exposition
November 17-22, 2002, New Orleans, Louisiana, USA

IMECE2002-DSC-32051

SIMULATION AND ANALYSIS OF TRANSIENT FUEL CELL SYSTEM PERFORMANCE BASED ON A DYNAMIC REACTANT FLOW MODEL

Jay T Pukrushpan **Huei Peng** **Anna G Stefanopoulou**
Automotive Research Center*
Department of Mechanical Engineering
University of Michigan
Ann Arbor, Michigan 48109-2125
Email: pukrushp@umich.edu

ABSTRACT

Fuel cell stack systems are under intensive development by several manufacturers since they complement heat engines and reduce the ubiquitous dependence on fossil fuels and thus have significant environmental and national security implications. To compete with ICE engines, however, fuel cell system must operate and function at least as well as conventional engines. Transient behavior is on of the key requirements for the success of fuel cell vehicles. The fuel cell system power response depends on the air and hydrogen feed, flow and pressure regulation, and heat and water management. During transient, the fuel cell stack control system is required to maintain optimal temperature, membrane hydration, and partial pressure of the reactants across the membrane in order to avoid degradation of the stack voltage, and thus, efficiency reduction. In this paper, we developed a fuel cell system dynamic model suitable for control study. The transient phenomena captured in the model include the flow characteristics and inertia dynamics of the compressor, the manifold filling dynamics (both anode and cathode), and consequently, the time-evolving reactant partial pressures, and membrane humidity. The effects of varying oxygen concentration and membrane humidity on the fuel cell voltage were included. Simulation results are presented to demonstrate the model capability.

*Support is provided by the U.S. Army Center of Excellence for Automotive Research, Contract DAAE07-98-3-0022

1 INTRODUCTION

Fuel Cells are electrochemical devices that convert the chemical energy of a gaseous fuel directly into electricity and are widely regarded as a potential alternative stationary and mobile power source. They complement heat engines and reduce the ubiquitous dependence on fossil fuels and thus have significant environmental and national security implications. Fuel cell stack systems are under intensive development by several manufacturers, with the Proton Exchange Membrane (PEM) Fuel Cells (also known as Polymer Electrolyte Membrane Fuel Cells) currently considered by many to be in a relatively more developed stage for ground vehicle applications. Recent announcements of GM "AUTOnomy" concept and federal program "Freedom CAR" confirm an interest in developing fuel cell vehicles from both the government and automobile manufacturers.

To compete with ICE engine, however, fuel cell system must operate and function at least as well as conventional engine. Transient behavior is one of the key requirements for the success of fuel cell vehicles. The fuel cell system power response depends on the air and hydrogen feed, flow and pressure regulation, and heat and water management. During transient, the fuel cell stack breathing control system is required to maintain optimal temperature, membrane hydration, and partial pressure of the reactants across the membrane in order to avoid degradation of the stack voltage, thus, maintain high efficiency and extend the life of the stack (Yang, 1998). Creating a control-oriented dynamic model of the overall system is an essential first step not only for the understanding of the system behavior but also for the

development and design of model-based control methodologies.

Model developed specifically for control studies have certain characteristics. Important characteristics such as dynamic (transient) effects are included while some other effects, such as spatial variation of parameters, are neglected and lumped. Furthermore, only dynamic effects that are related to automobile operations are integrated into the model. The extremely fast transient phenomena of both electrochemical reaction and electrode electrical dynamics have minimal effects in automobile application and can be neglected. The transient behavior due to manifold filling dynamics, membrane water content, supercharging devices, and temperature may impact the behavior of the vehicle (Guzzella, 1999), and thus must be included in the model. Interactions between each of these processes must also be included. However, with relatively slow responses, the cell and stack temperature may be viewed as a separate system which is equipped with its own controller. The temperature can then be considered as a constant for other faster subsystems.

Despite a large number of publications on fuel cell modeling, models of fuel cell systems suitable for control studies are still lacking. Most publications target the fuel cell performance prediction with the main purpose of designing cell components and choosing fuel cell operating points (Amphlett, 1995; Bernardi, 1992; Lee, 1998; Springer, 1991) . These models are mostly steady-state, cell level, include spatial variations of fuel cell parameters and are developed using electrochemical, thermodynamic and fluid mechanics. While these models are not suitable for control studies, they explain the fundamental effects of operating parameters on the fuel cell voltage or polarization curve. Fuel cell (propulsion) system models that exist in the literature are mostly steady-state system models which typically used for component sizing (Barbir, 1999; Friedman, 2001) and cumulative fuel consumption or hybridization studies (Akella, 2001; Atwood, 2001; Boettner, 2001b). Here, each component such as compressor, heat exchanger and fuel cell stack voltage is represented by a static performance or efficiency map. The only dynamics considered in this type of models is the vehicle inertia.

Very few dynamic fuel cell system models exist in the open literature. Most of them are built to address specific control problems and include only the subsystems relevant to the control problem. The temperature dynamics is the focus of several publication (Turner, 1999; Boettner, 2001a; Hauer, 2000) because of the critical startup period where nominal fuel cell temperature needs to be reached fast. A few publications (Guzzella, 1999; Padulles, 1999; Pischinger, 2001) included the dynamics of the air supply system, i.e., considered the dynamics of the air compressor and manifold filling and their consequences to the fuel cell system behavior.

In this paper, we developed a fuel cell system dynamic model suitable for control study. The transient phenomena captured in the model include the flow characteristics and inertia dynamics of the compressor, the manifold filling dynamics (both anode and cathode), and consequently, the time-evolving reactant partial pressures, and membrane humidity. All these dynamically changing conditions affect the fuel cell stack voltage, and thus, the fuel cell efficiency and power. Unlike other system models existing in the literature where a single polarization curve or a set of polarization curves for different cathode pressure is used, the fuel cell polarization curve used in this paper is a function of oxygen and hydrogen partial pressures and membrane water content. This allows us to capture the effects of varying oxygen concentration and membrane humidity on the fuel cell voltage, which is necessary for control development during transient operation. Simulation results are presented to demonstrate the model capability.

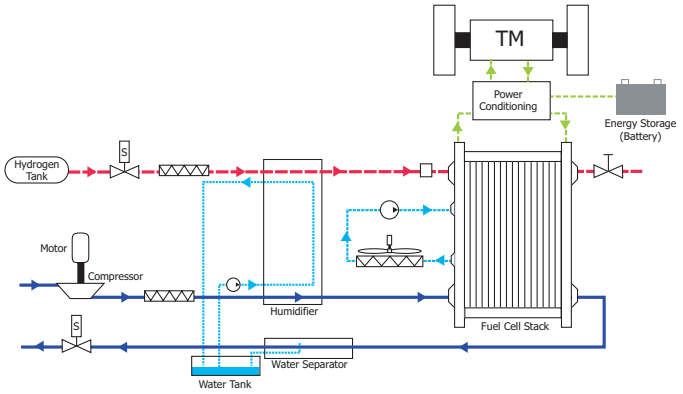

Figure 1. Automotive Fuel Cell Propulsion System

2 FUEL CELL PROPULSION SYSTEM FOR AUTOMOBILE

A fuel cell stack needs to be integrated with other components to form a fuel cell engine. The diagram in Figure 1 shows the components required for the fuel cell system. The fuel cell stack requires four flow systems: (i) hydrogen supply system (ii) air supply system (iii) cooling system and (iv) humidification system. Most fuel cell stacks use de-ionized water as a coolant and the cooling system and humidification system can often be combined as a water supply system.

The power of the fuel cell stack depends on current drawn from the stack and stack voltage. The fuel cell voltage is a function of the current, reactant partial pressure, temperature and membrane humidity. As the current is drawn from the fuel cell, oxygen and hydrogen are used in the reaction. Water and heat are also generated. To maintain the desired hydrogen partial pressure, the hydrogen needs to be replenished by the hydrogen supply system, which includes hydrogen pressurized tank and hydrogen control valve. Similarly, the air supply system needs to replenish the oxygen to maintain the oxygen partial pressure. The air supply system is composed of compressor, electric motor and pipe between the components. The compressor compress the

air flow to high pressure which significantly improves the reaction rate, and thus fuel cell efficiency and power density. Since the high pressure air flow leaving the compressor has high temperature, air cooler is needed to reduce air temperature entering the stack. Humidifier is also used to humidify the air and hydrogen flow in order to prevent dehydration of the fuel cell membrane. The water used in the humidifier is supplied from the water tank. Water level in the tank needs to be maintained by collecting water generated in the stack, which is carried out with the air flow. The excessive heat released in the fuel cell reaction also needs to be removed by the cooling system, which re-circulates de-ionized water through the fuel cell stack. Power conditioner is frequently needed since the voltage of fuel cell stack varies significantly, which is not suitable for typical electronic components or traction motors. The stack power is supplied to the traction motor that is connected to the vehicle drivetrain.

3 FUEL CELL SYSTEM MODEL

In this study, the problem is simplified by assuming that the temperature and humidity of the inlet reactant flow can be perfectly controlled, i.e. assuming perfectly controlled humidifier and heat exchanger. Simple models of air cooler and humidifier are used to calculate changes in flow conditions in order to ensure mass conservation of various species.

The component and the volumes associated with the system are shown in Figure 2. It is assumed that the multiple cathode and anode volumes of the multiple fuel cells in the stack are lumped together as a single stack cathode and anode volumes. The anode supply and return manifold volumes are very small and the pure hydrogen flow allows us to lump all these volumes to one "anode" volume. We denote all the variables associated with the lumped anode volume with a subscript (*an*). Similarly, the cathode supply manifold (*sm*) lumps all the volumes associated with pipes and connection between the compressor and the stack cathode (*ca*) flowfield. The cathode return manifold (*rm*) represents lump volume of pipes downstream of the stack cathode. It is assumed that the properties of the flow exiting a volume is the same as that of the gas inside the volume. Subscripts (*cp*) and (*cm*) are used for compressor and compressor motor, respectively.

The inertia dynamic and nonlinear curve-fitting of the compressor flow map are used to model the compressor. The mass conservation is used to model dynamic behavior of gas species in each volume. If there is no variation of gas composition in a volume, the mass conservation is applied to the combined gas, for example, in the supply and return manifolds. The energy conservation is applied to the air in the supply manifold in order to account for the effect of temperature variations. The parameters used in the model, given in Table 3, are either taken from the literature or approximated based on the dimensions of Ford P2000 fuel cell vehicle.

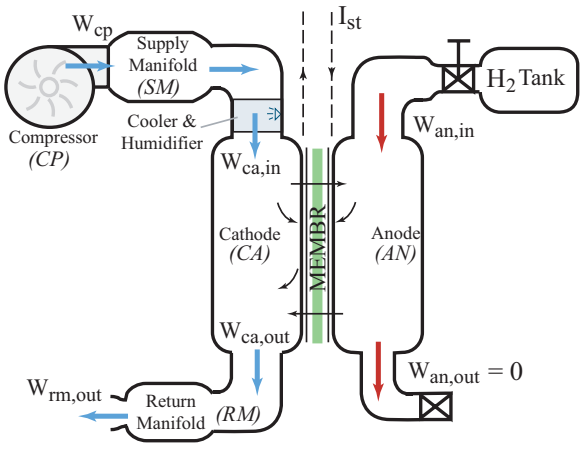

Figure 2. Components and volumes in fuel cell reactant supply system

3.1 Compressor Model

A lumped rotational parameter model with inertia, J_{cp}, is used to represent the dynamic behavior of the compressor speed, ω_{cp}.

$$J_{cp}\frac{d\omega_{cp}}{dt} = (\tau_{cm} - \tau_{cp}) \tag{1}$$

where $\tau_{cm}(v_{cm}, \omega_{cp})$ is the compressor motor (CM) torque and τ_{cp} is the required compressor torque in (3). The compressor motor torque is calculated using static motor equation

$$\tau_{cm} = \eta_{cm}\frac{k_t}{R_{cm}}(v_{cm} - k_v\omega_{cp}) \tag{2}$$

where k_t, R_{cm} and k_v are motor constants and η_{cm} is the motor mechanical efficiency. The required motor torque is calculated using thermodynamic equation

$$\tau_{cp} = \frac{C_p}{\omega_{cp}}\frac{T_{atm}}{\eta_{cp}}\left[\left(\frac{p_{sm}}{p_{atm}}\right)^{\frac{\gamma-1}{\gamma}} - 1\right]W_{cp} \tag{3}$$

where γ is air specific heat ratio, C_p is air specific heat, η_{cp} is compressor efficiency, p_{sm} is pressure inside the supply manifold and p_{atm} and T_{atm} are atmospheric pressure and temperature, respectively.

A static compressor map is used to determine the air flow rate through the compressor, W_{cp}. The compressor flow characteristic $W_{cp}(p_{sm}/p_{atm}, \omega_{cp})$ is modeled by the Jensen & Kristensen nonlinear curve fitting method (Moraal, 1999), which represents the compressor data very well as shown in Figure 3. The compressor model used here is for an Allied Signal compressor (Cunningham, 1999). Thermodynamic equations are used to calculate the exit air temperature.

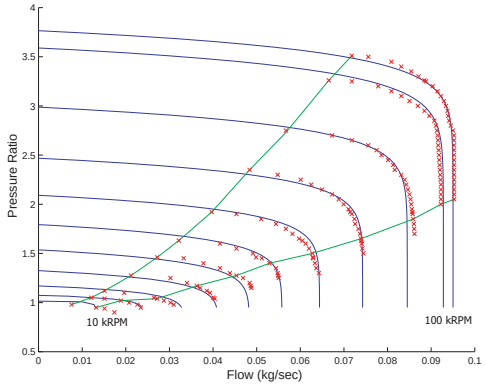

Figure 3. Compressor Map

$$T_{cp} = T_{atm} + \frac{T_{atm}}{\eta_{cp}} \left[\left(\frac{p_{sm}}{p_{atm}} \right)^{\frac{\gamma-1}{\gamma}} - 1 \right] \tag{4}$$

3.2 Supply Manifold Model

Manifold model represents lumped volume associated with pipes and connections between each device. The cathode supply manifold (SM) includes pipe volume between compressor and fuel cell stack. The pressure in the supply manifold, p_{sm}, is governed by mass continuity equation and energy conservation

$$\frac{dm_{sm}}{dt} = W_{cp} - W_{sm,out} \tag{5}$$

$$\frac{dp_{sm}}{dt} = \frac{\gamma R_a}{V_{sm}} \left(W_{cp} T_{cp} - W_{sm,out} T_{sm} \right) \tag{6}$$

where R_a is the air gas constant, V_{sm} is the supply manifold volume and T_{sm} is the temperature of the flow inside the manifold which is calculated from the ideal gas law. The supply manifold exit flow, $W_{sm,out}(p_{sm}, p_{ca})$, is calculated using a linearized nozzle flow equation (34), given in Appendix A.

3.3 Static Air Cooler Model

The temperature of the air in the supply manifold is typically high due to the high temperature of air leaving the compressor. To prevent any damage to the fuel cell membrane, the air needs to be cooled down to stack operating temperature. In this study, we do not address heat transfer effects and thus we assume that an ideal air cooler (CL) maintains the temperature of the air entering the stack at $T_{cl} = 80°C$. It is assumed that there is no pressure drop in the cooler, $p_{cl} = p_{sm}$. Since temperature change effects gas humidity, the humidity of the gas exiting the cooler is calculated

$$\phi_{cl} = \frac{p_{v,cl}}{p_{sat}(T_{cl})} = \frac{p_{cl} p_{v,atm}}{p_{atm} p_{sat}(T_{cl})} = \frac{p_{cl} \phi_{atm} p_{sat}(T_{atm})}{p_{atm} p_{sat}(T_{cl})} \tag{7}$$

where $\phi_{atm} = 0.5$ is the average ambient air relative humidity and $p_{sat}(T_i)$ is the vapor saturation pressure that is a function of temperature, T_i.

3.4 Static Humidifier Model

It is also assumed that the inlet air is humidified to the desired relative humidity before entering the stack. A static model of the humidifier is used to calculate the required water that needs to be injected to the flow stream. The temperature of the flow is assumed constant. The water injected is assumed to be in the form of vapor or the latent heat of vaporization is assumed to be taken into account in the air cooler. The amount of vapor injected is calculated by comparing the vapor flow at the cooler outlet and the required vapor flow for the desired humidity, ϕ^{des}. First, based on the condition of the flow exiting the cooler ($W_{cl} = W_{sm,out}, p_{cl}, T_{cl}, \phi_{cl}$), the dry air mass flow rate, $W_{a,cl}$, the vapor mass flow rate, $W_{v,cl}$ and the dry air pressure, $p_{a,cl}$, are calculated using equations (35)-(39). Then, the flow rate of vapor injected is calculated by

$$W_{v,inj} = \frac{M_v}{M_a} \frac{\phi^{des} P_{sat}(T_{cl})}{p_{a,cl}} W_{a,cl} - W_{v,cl} \tag{8}$$

where M_v and M_a are molar mass of vapor and dry air, respectively. The cathode inlet flow rate and pressure are $W_{ca,in} = W_{cl} + W_{v,inj}$ and $p_{ca,in} = p_{a,cl} + \phi^{des} p_{sat}(T_{cl})$, respectively.

3.5 Fuel Cell Stack Model

The fuel cell stack (ST) model contains four interacting submodels which are the stack voltage, the anode flow, the cathode flow, and the membrane hydration models (Figure 4). Currently, it is assumed that the temperature of the fuel cell stack is perfectly controlled by the cooling system such that its temperature is maintained constant at $80°C$ and uniform over the whole stack and across the flowfield. The voltage model contains an equation used to calculate stack voltage that depends on varying fuel cell variables: pressure, temperature, reactant gas partial pressures and membrane humidity. The dynamically varying pressure and relative humidity of the reactant gas flow inside the stack flow channels are calculated in the cathode and the anode flow model using mass conservation along with the thermodynamic properties. The process of water transfer across the membrane is represented by the membrane hydration model.

3.5.1 Stack Voltage Model In the stack voltage model, the stack voltage is calculated as a function of stack current, cathode pressure, reactant partial pressures, fuel cell temperature and membrane humidity. Since the fuel cell stack comprises of multiple fuel cell connected in series, the stack voltage, v_{st}, is calculated by multiplying the cell voltage, v_{fc}, by the number of cells, n, in the stack ($v_{st} = n v_{fc}$). The stack current, I_{st}, is

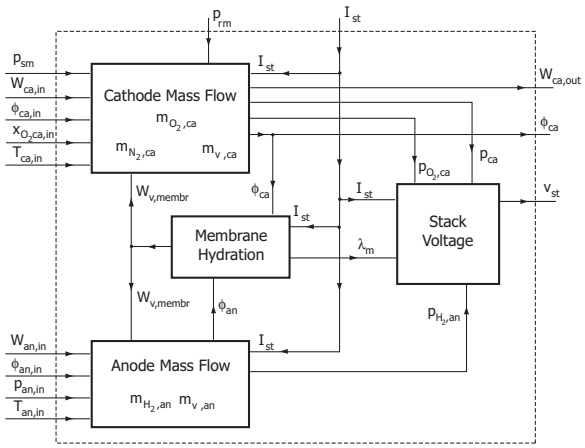

Figure 4. Fuel Cell Stack Block Diagram

equal to the cell current. For a set of fuel cell operating conditions (pressures, temperature and humidity) the characteristic of fuel cell is typically given in the form of polarization curve, which is a plot of cell voltage, v_{fc}, and cell current density, i_{fc} (see Figure 5 for an example). The current density is defined as cell current per unit of cell active area, $i_{fc} = I_{st}/A_{fc}$.

The fuel cell voltage is calculated using a combination of physical and empirical relationships. Basic explanation can be found in (Larminie, 2000). In summary, the fuel cell voltage is given by

$$v_{fc} = E - v_{act} - v_{ohm} - v_{conc} \tag{9}$$

where E is the open circuit voltage and v_{act}, v_{ohm} and v_{conc} are activation, ohmic and concentration overvoltages, respectively. The open circuit voltage is calculated from the energy balance between chemical energy in the reactants and electrical energy and is derived in (Amphlett, 1995)

$$E = 1.229 - 0.85 \times 10^{-3}(T_{fc} - 298.15) + 4.3085 \times 10^{-5} T_{fc} \left[\ln(p_{H_2}) + \frac{1}{2}\ln(p_{O_2}) \right] \tag{10}$$

where, specifically in (10), fuel cell temperature T_{fc} is expressed in Kelvin, and reactant partial pressures p_{H_2} and p_{O_2} are expressed in atm.

Activation overvoltage, v_{act}, is the result of the need to cause electron transfer and to break and form chemical bonds in the anode and cathode (Lee, 1998). The relation between the activation overvoltage and the current density is described by the Tafel equation which is however not valid for small current density. Therefore, the Tafel equation is approximated by expression

$$v_{act} = v_0 + v_a(1 - e^{-c_1 i}). \tag{11}$$

The activation overvoltage depends strongly on temperature (Kordesch, 1996) and oxygen partial pressure (Amphlett, 1995). The value of v_0, v_a and c_1 and their dependency on oxygen partial pressure and temperature can be determined from nonlinear regression of experimental data using the basis function (11).

Ohmic overvoltage, v_{ohm}, is due to the resistance of the polymer membrane to the transfer of protons and the resistance of the electrode and collector plate to the transfer of electrons. The voltage drop that corresponds to the ohmic loss is proportional to the current density

$$v_{ohm} = i \cdot R_{ohm}. \tag{12}$$

The ohmic resistance, R_{ohm}, depends strongly on membrane humidity (Laurencelle, 2001) and cell temperature (Amphlett, 1994). Several studies in the literature (Nguyen, 1993; Springer, 1991) show that the ohmic resistance is a function of the membrane conductivity, $\sigma_m(\lambda_m, T_{fc})$ $(\Omega \cdot \mathrm{cm})^{-1}$, in the form

$$R_{ohm} = \frac{t_m}{\sigma_m}, \tag{13}$$

where t_m is the membrane thickness. The value of membrane water content, λ_m, varies between 0 and 14 (Springer, 1991), which is equivalent to relative humidity (RH) of 0% and 100%, respectively. The variation of the membrane conductivity with different membrane humidity and pressure is in the form (Springer, 1991)

$$\sigma_m = (b_{11}\lambda_m - b_{12}) \exp\left(b_2 \left(\frac{1}{303} - \frac{1}{T_{fc}} \right) \right) \tag{14}$$

where λ_m is the membrane water content, b_{11}, b_{12} and b_2 are constants, which are usually determined empirically. We use the empirical values of b_{11} and b_{12} for Nafion 117 membrane given in (Springer, 1991).

Concentration overvoltage, v_{conc}, results from the change in concentration of the reactants as they are consumed in the reaction. An equation that approximates the voltage drop from concentration losses is given by (Guzzella, 1999)

$$v_{conc} = i \left(c_2 \frac{i}{i_{max}} \right)^{c_3} \tag{15}$$

where c_2, c_3 and i_{max} are constants that depend on temperature and reactant partial pressure and can be determined empirically.

We use the published values for the coefficients t_m and b_1 in (13) and (14). The value of $b_2 = 350$ is however modified from the one given in (Springer, 1991) to better match the experiment data. The coefficients in the expression (11) and (15) are determined using nonlinear regression with fuel cell polarization data from an automotive propulsion sized PEM fuel cell stack. By assuming that the data is obtained from the fuel cell stack operating in controlled environment, where cathode gas is fully humidified

and oxygen excess ratio (ratio of oxygen supplied to oxygen reacted) is 2, the pressure terms in the regression of the activation and concentration overvoltage can be related to oxygen partial pressure, p_{O_2}, and vapor saturation pressure, p_{sat}. The resulting voltage equation is therefore expressed as a functions of oxygen partial pressure. The regression results are

$$
\begin{aligned}
v_0 &= 0.279 - 8.5\times10^{-4}(T_{fc}-298.15) \\
&\quad +4.308\times10^{-5}T_{fc}\left[\ln\left(\frac{p_{ca}-p_{sat}}{1.01325}\right)\right. \\
&\quad \left.+\frac{1}{2}\ln\left(\frac{0.1173(p_{ca}-p_{sat})}{1.01325}\right)\right] \\
v_a &= (-1.618\times10^{-5}T_{fc}-1.618\times10^{-2})(\frac{p_{O_2}}{0.1173}+p_{sat})^2 \\
&\quad +(1.8\times10^{-4}T_{fc}-0.166)(\frac{p_{O_2}}{0.1173}+p_{sat}) \\
&\quad +(-5.8\times10^{-4}T_{fc}+0.5736) \\
c_1 &= 10 \\
c_2 &= \begin{cases} (7.16\times10^{-4}T_{fc}-0.622)(\frac{p_{O_2}}{0.1173}+p_{sat}) \\ \quad +(-1.45\times10^{-3}T_{fc}+1.68) \\ \quad \text{for } (\frac{p_{O_2}}{0.1173}+p_{sat}) < 2 \text{ atm} \\ (8.66\times10^{-5}T_{fc}-0.068)(\frac{p_{O_2}}{0.1173}+p_{sat}) \\ \quad +(-1.6\times10^{-4}T_{fc}+0.54) \\ \quad \text{for } (\frac{p_{O_2}}{0.1173}+p_{sat}) \geq 2 \text{ atm} \end{cases} \\
i_{max} &= 2.2 \\
c_3 &= 2
\end{aligned}
\tag{16}
$$

The plot of the polarization function versus the experimental

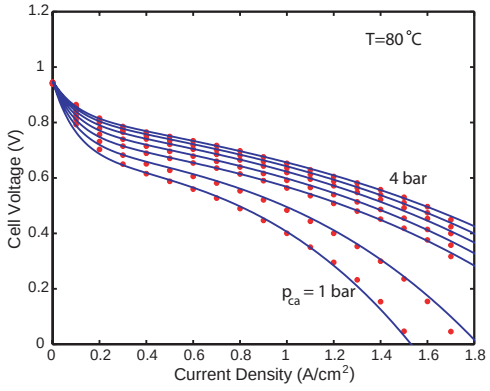

Figure 5. Fuel cell polarization curve fitting results at constant temperature of $80^{\circ}C$ and at cathode pressure of [1, 1.5, 2, 2.5, 3, 3.5, 4] bar

data is shown in Figure 5. An example of the effect of membrane water content to cell voltage is illustrated in Figure 6 which shows fuel cell polarization curve for membrane water content of 14 (100%) and 7 (50%). Unfortunately, there is no experimental data to verify the relation in Figure 6 but one can see that the model predicts significant degradation in fuel cell voltage due to change in the membrane water content indicating the importance of experimental verification. Note also that over saturated

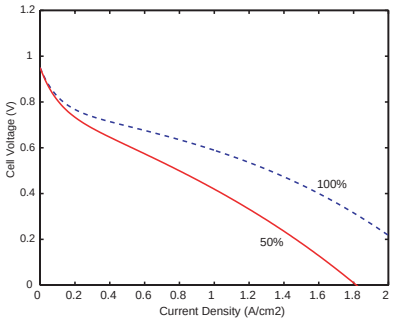

Figure 6. Polarization curves for $100^{\circ}C$ and 2.5 bar at different membrane water content

conditions will cause condensation and liquid formulation inside the anode or the cathode. The flooding will also cause voltage degradation (Baschuk, 2000). The effect of water flooding will be integrated into our model in the future.

3.5.2 Cathode Flow Model The cathode (CA) mass flow model represents the air flow behavior inside the cathode flow channel of the fuel cell. The model is developed using the mass conservation principle and thermodynamic and psychrometric properties of air. Several assumptions are used. First, all gases obey the ideal gas law. The temperature of the flow inside the cathode flow channel is assumed to be equal to the stack temperature. The variables of the flow exiting a volume such as temperature, pressure, and humidity are assumed to be the same as the variables inside the upstream volume. Furthermore, when the relative humidity of the gas exceeds 100%, vapor condenses into liquid form. This liquid water does not leave the stack and will either evaporate in the cathode gas if its humidity drops below 100% or accumulate in the cathode. Lastly, the flow channel and cathode backing layer are lumped into one volume, i.e. the spatial variations are ignored.

The mass continuity is used to balance the mass of three elements, which are oxygen, nitrogen and water, inside the cathode volume.

$$\frac{dm_{O_2}}{dt} = W_{O_2,in} - W_{O_2,out} - W_{O_2,reacted} \tag{17}$$

$$\frac{dm_{N_2}}{dt} = W_{N_2,in} - W_{N_2,out} \tag{18}$$

$$\frac{dm_{w,ca}}{dt} = W_{v,ca,in} - W_{v,ca,out} + W_{v,gen} + W_{v,membr} \qquad (19)$$

Using the mass of oxygen, m_{O_2}, nitrogen, m_{N_2}, and water, m_w, and the stack temperature, T_{st}, oxygen, nitrogen and vapor partial pressure, p_{O_2}, p_{N_2}, p_v, cathode total pressure, $p_{ca} = p_{O_2} + p_{N_2} + p_v$, relative humidity, ϕ_{ca}, and dry air oxygen mole fraction, $x_{O_2,ca}$, of the gas inside the cathode channel can be calculated using the ideal gas law and thermodynamic properties. If the mass of water calculated is more than that of saturated state, the extra amount is assumed to condense into liquid form instantaneously. Figure 7 illustrates the calculation process in the cathode model.

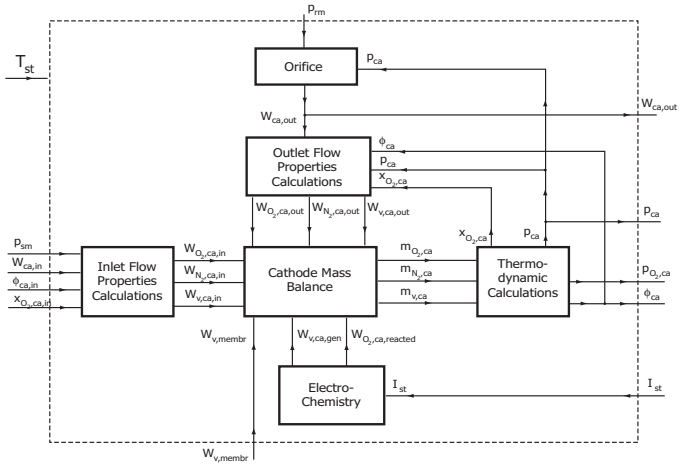

Figure 7. Cathode Flow Model

The inlet (*in*) and outlet (*out*) mass flow rate of oxygen, nitrogen and vapor in equation (17)-(19) are calculated from the inlet and outlet cathode flow conditions using thermodynamic properties. The detailed calculations are given in Appendix A. A linearized nozzle equation (34) is used to calculate the cathode exit flow rate, $W_{ca,out}$. Electrochemistry principles are used to calculate the rates of oxygen consumption, $W_{O_2,reacted}$, and water production, $W_{v,ca,gen}$, in the fuel cell reaction. The flow rates are functions of the stack current, I_{st} (Amp),

$$W_{O_2,reacted} = M_{O_2} \times \frac{nI_{st}}{4F} \qquad (20)$$

$$W_{v,ca,gen} = M_v \times \frac{nI_{st}}{2F} \qquad (21)$$

The water flow rate across the membrane, $W_{v,membr}$, in (19) is calculated by the membrane hydration model in section 3.5.4.

3.5.3 Anode Flow Model Similar to the cathode flow model, hydrogen partial pressure and anode flow humidity are determined by balancing the mass flow of hydrogen, m_{H_2}, and water in the anode, $m_{w,an}$.

$$\frac{dm_{H_2}}{dt} = W_{H_2,in} - W_{H_2,out} - W_{H_2,reacted} \qquad (22)$$

$$\frac{dm_{w,an}}{dt} = W_{v,an,in} - W_{v,an,out} - W_{v,membr} \qquad (23)$$

In our model, pure hydrogen gas is supplied to the anode of the fuel cell stack by the hydrogen tank. It is assumed that the anode inlet flow rate can be instantaneously adjusted by a valve such that it maintains minimum pressure difference across the membrane. This has been achieved by using a high gain proportional controller to control the hydrogen flow rate such that the anode pressure, p_{an}, tracks the cathode pressure, p_{ca}. The inlet hydrogen flow is assumed to have 100% relative humidity. The anode outlet flow represents the hydrogen purge and is currently assumed to be zero. The temperature of the flow is assumed to be equal to the stack temperature. The rate of hydrogen consumed in the reaction, $W_{H_2,reacted}$, is a function of the stack current

$$W_{H_2,reacted} = M_{H_2} \times \frac{nI}{2F} \qquad (24)$$

where M_{H_2} is hydrogen molar mass.

3.5.4 Membrane Hydration Model The membrane hydration model captures the effect of the water content in the membrane and the rate of mass flow of water across the membrane. Both water content and mass flow are assumed to be uniform over the surface area of the membrane. The membrane water content and rate of mass flow across the membrane are functions of the stack current and relative humidity of the gas inside the anode and cathode flow channels.

The water transport across membrane is achieved through two distinct phenomena (Nguyen, 1993; Springer, 1991). First, the electro-osmotic drag phenomenon is responsible for the water molecules dragged across the membrane from anode to cathode by the hydrogen proton. The amount of water transported is represented by the electro-osmotic drag coefficient, n_d, which is defined as number of water molecules carried by each proton. Second, the gradient of water concentration across the membrane due to the difference in humidity in anode and cathode gases causes "back-diffusion" of water from cathode to anode. We approximate the water concentration, c_v, gradient in the membrane to be linear over the membrane thickness, t_m. Combining the two water transports, the water flow across the membrane can be written as (assuming positive in the direction from anode to cathode)

$$W_{v,membr} = M_v A_{fc} n \left(n_d \frac{i}{F} - D_w \frac{(c_{v,ca} - c_{v,an})}{t_m} \right). \qquad (25)$$

The coefficients n_d and D_w vary with water content in the membrane, λ_m, which depends on the water content in the gas next to the membrane.

The membrane water content, λ_m, is calculated using the membrane water activity, a_m, which is an average of water activities of the gas in the anode and the cathode, $a_i = x_{v,i}p_i/p_{sat,i} = p_{v,i}/p_{sat,i}$, $i = [an, ca]$:

$$\lambda_i = \begin{cases} 0.043 + 17.81a_i - 39.85a_i^2 + 36.0a_i^3 & , 0 < a_i \leq 1 \\ 14 + 1.4(a_i - 1) & , 1 < a_i \leq 3. \end{cases} \quad (26)$$

Note that in the case of gas the water activity, a_i, is equal to the relative humidity ϕ_i. The electro-osmotic and diffusion coefficients are calculated by

$$n_d = 0.0029\lambda_m^2 + 0.05\lambda_m - 3.4 \times 10^{-19} \quad (27)$$

and

$$D_w = D_\lambda \exp\left(2416\left(\frac{1}{303} - \frac{1}{T_{fc}}\right)\right) \quad (28)$$

where

$$D_\lambda = \begin{cases} 10^{-6} & , \lambda_m < 2 \\ 10^{-6}(1 + 2(\lambda_m - 2)) & , 2 \leq \lambda_m \leq 3 \\ 10^{-6}(3 - 1.67(\lambda_m - 3)) & , 3 < \lambda_m < 4.5 \\ 1.25 \times 10^{-6} & , \lambda_m \geq 4.5 \end{cases} \quad (29)$$

and T_{fc} is the fuel cell temperature. The water concentration at the membrane surfaces, $c_{v,an}$ and $c_{v,ca}$, are functions of water content on the surface, λ_{an} and λ_{ca}, specifically, $c_{v,i} = \frac{\rho_{m,dry}}{M_{m,dry}}\lambda_i$, $i = [an, ca]$ where $\rho_{m,dry}$ (kg/cm^3) is the membrane dry density and $M_{m,dry}$ (kg/mol) is the membrane dry equivalent weight. The surface water contents λ_{an} and λ_{ca} are calculated using equation (26) from a_{an} and a_{ca}, respectively. These equations are developed based on experimental results measured for Nafion 117 membrane in (Springer, 1991).

4 Return Manifold Model

Unlike the supply manifold where temperature changes need to be accounted, the temperature in the return manifold, T_{rm}, is assumed constant and equal to the temperature of the flow leaving the cathode. The return manifold pressure, p_{rm}, is governed by the mass conservation and the ideal gas law through isothermic assumptions.

$$\frac{dp_{rm}}{dt} = \frac{R_a T_{rm}}{V_{rm}}(W_{ca,out} - W_{rm,out}) \quad (30)$$

The nonlinear nozzle equations (32)-(33) are used to calculate the return manifold exit air flow rate, $W_{rm,out}$, as a function of the return manifold pressure and back-pressure valve opening area, A_T.

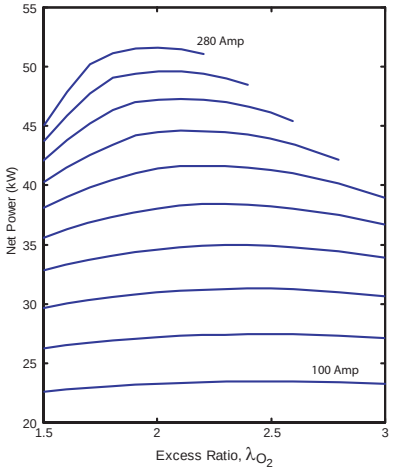

Figure 8. System net power at different stack current and oxygen excess ratio

5 Analysis

The net power, P_{net}, of the fuel cell system is the difference between the power produced by the stack, P_{st}, and the parasitic power required to run the auxiliary components. The majority of the parasitic power is caused by the air compressor. Therefore, it is the only parasitic loss considered in this study. For certain stack current, the stack voltage increases with increasing air flow rate to the stack since the cathode oxygen partial pressure increases. The excess amount of air flow provided to the stack is normally indicated by the term oxygen excess ratio, λ_{O_2}, defined as a ratio of oxygen supplied to oxygen used in the cathode, i.e. $W_{O_2,in}/W_{O_2,ract}$. High oxygen excess ratio, and thus high oxygen partial pressure, improves P_{st} and P_{net}. However, after an optimum value of λ_{O_2}, further increase will cause excessive increase of compressor power and thus deteriorate the system net power. To study the optimal value of λ_{O_2}, we plot steady-state values of λ_{O_2} and P_{net} for different I_{st} as shown in Figure 8 . For the current fuel cell system, the highest net power is achieved at an oxygen excess ratio between 2 and 2.4 depending on the stack current. It is therefore desired to control the air flow to $\lambda_{O_2} = 2$.

The parameter values that represent the effect of membrane humidity to the fuel cell voltage in equations (13) and (14) are obtained from the existing literature and it corresponds to different membrane from the one used in the fuel cell considered in this paper. Using these coefficients in the model results in dehydration of anode side. It is therefore more reasonable to assume that there is another way to humidify the membrane and consider only the effect of air supply system with the membrane fully hydrated. This is an appropriate assumption since there are industrial efforts to redesign the fuel cell components to address the membrane humidity problem by passive means. It is also assumed that the anode and cathode flow enter the stack at 100%RH and 50%RH, respectively, and both are at 80°C.

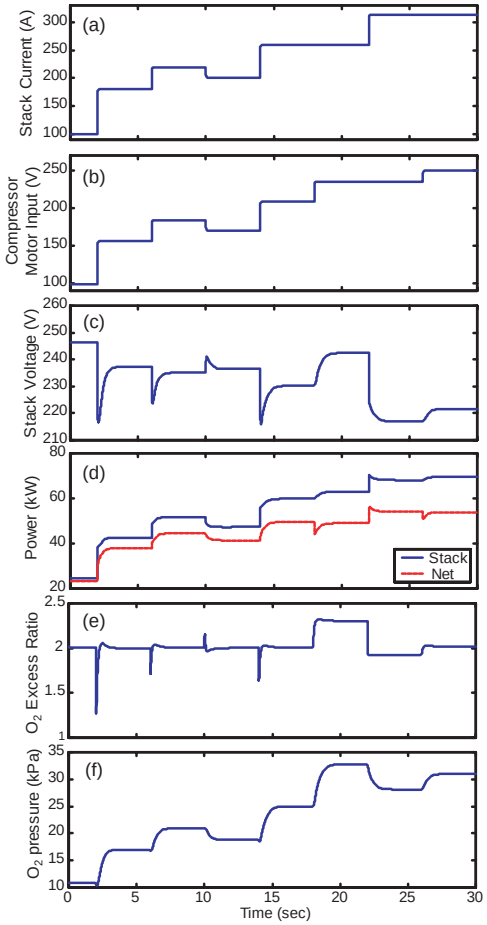

Figure 9. Simulation results of the fuel cell system model for a series of input step change

The results of simulation of vehicle propulsion sized (75 kW) fuel cell system are shown in Figures 9-10. A series of step changes in stack current is applied as an input (Figures 9(a)). A series of compressor motor input voltage (Figures 9(b)) that give different level of steady-state oxygen excess ratio (Figures 9(e)) is also applied. During a possitive current step, oxygen excess ratio drops (Figures 9(e)) due to depletion of oxygen. This, in turn, causes significant drop in the stack voltage as shown in Figures 9(c). If the compressor voltage responses instantaneously during current step (at 2, 6, 10 and 14 seconds), there is still a transient effect in the stack voltage, and consequently in the stack power and net power (Figures 9(c)), as a result of the transient behavior in oxygen partial pressure (Figures 9(f)). The step at time 18 second shows the response of stepping the compressor input while keeping constant stack current. An opposite case is shown at the time 22 second. The steady-state response at 16 and 20 seconds show the effect of running the system at λ_{O_2} higher than optimum value. It can be seen in Figures 9(c) that even though the stack power increases, the net power decreases due to the high power drawn from the compressor motor. Figure 10 shows the fuel cell response on the polarization map at $80\,^{\circ}C$. Similar result is obtained in the experiment of fuel cell load switching presented in (Laurencelle, 2001). Figure 11 shows the voltage response when consider the humidity of the membrane.

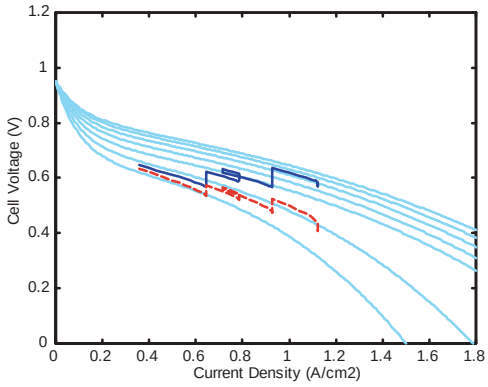

Figure 10. Fuel cell response on polarization curve. Solid line assumes fully humidified membrane. Dashed line represents drying membrane

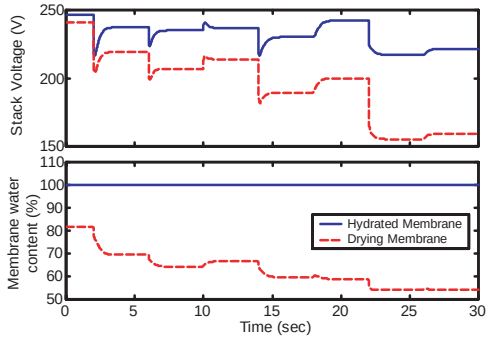

Figure 11. Voltage response comparing fully humidified membrane and drying membrane

A transient step change in stack current requires rapid increase in air flow to prevent depletion of cathode oxygen. This requires a large amount of power drawn by the compressor motor and thus increases parasitic loss, which affects the system net power. A control problem can be formulated by defining design objective to control the compressor motor voltage, v_{cm}, in order to reduce λ_{O_2} excursions from the desired $\lambda_{O_2}^{des} = 2$ and achieve the desired system net power transient response. Figure 12 shows the control problem formulation. The stack current is viewed as an external input. The control input is the compressor motor voltage. The two performance variables are λ_{O_2} and P_{net}. Measurements include compressor flow rate, supply manifold pressure and stack voltage. The nonlinear model is lin-

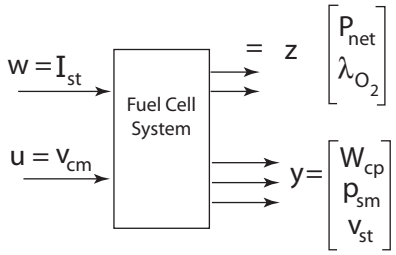

Figure 12. Control Problem Formulation

earized around 40 kW net power according to the input-output in Figure 12. The resulting linear system exhibits a non-minimum phase (NMP) relation between the input v_{cm} and the output P_{net}. This corresponds to the fact that compressor motor is powered by the fuel cell stack, Figure 13. The non-minimum phase relation limits the performance of the control and results in transient tradeoff between λ_{O_2} and P_{net}, as studied in (Pukrushpan, 2002). Furthermore, the location of NMP zero varies for different system operating points as illustrated in Table 1 for different net power and Table 2 for different oxygen excess ratio. This variation needs to be taken into account when ones use linear control techniques to develop system controllers. In Table 2, as we increase the oxygen excess ratio over the optimal value (illustrated in Figure 8), the linearization results in a minimum phase system with negative gain (in dB). This change in behavior is due to deteriorating effect of excessive compressor power.

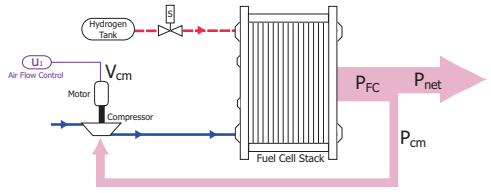

Figure 13. Schematic of the underlying principle behind the non-minimum phase behavior

Table 1. Location of NMP zeros at different operating net power and for constant oxygen excess ratio $\lambda_{O_2} = 2$

P_{net} (kW)	30	38	40	41	42	45	50
z_{NMP}	0.55	0.63	0.64	0.69	0.27	0.19	0.12

6 CONCLUSION

Models of main components of control-oriented fuel cell system model have been developed using physical principle and simulation results are presented. The transient phenomena of flow characteristics and inertia dynamics of the compressor, manifold filling dynamics and time-evolving reactant partial pressure and membrane humidity are captured.

The parameter values used in the model are obtained from publications but there is little information on experimental transient behavior of fuel cell or fuel cell systems. With additional experimental results, the coefficients can be adjusted and the model will be able to more accurately representing a real fuel cell system. The model, although, not fully validated, it captures the intrinsic breathing dynamics of pressurized fuel cell stack. Transient experimental data will be used in the future to calibrate the membrane hydration constants and develop a model representing the effect of membrane water flooding.

Table 2. Location of NMP zeros at different λ_{O_2} ($I_{st} = 190A$)

λ_{O_2}	NMP zero	DC Gain (dB)
1.5	1.81	0.113
1.8	1.06	0.074
2.0	0.63	0.049
2.1	0.14	0.011
2.2	n/a	-0.001
2.5	n/a	-0.030

Table 3. Model parameters

Variables	Value	Variables	Value
n	381 cells	$\rho_{m,dry}$	0.002 kg/cm^3
A_{fc}	280 cm^2	$M_{m,dry}$	1.1 kg/mol
V_{an}	0.005 m^3	t_m	0.01275 cm
V_{ca}	0.01 m^3	J_{cp}	5×10^{-5} kg-m^2
V_{sm}	0.02 m^3	$k_{sm,out}$	0.36×10^{-5} kg/(s·Pa)
V_{rm}	0.005 m^3	$k_{ca,out}$	0.22×10^{-5} kg/(s·Pa)
$C_{D,rm,out}$	0.011	$A_{T,rm,out}$	0.002 m^2

ACKNOWLEDGMENT

We thank the Automotive Research Center at the University of Michigan for the funding support. We also thank Herb Dobbs and Erik Kallio at TACOM and Woong-Chul Yang and James Adams at Ford Motor Company for their advice.

REFERENCES

J.A. Adams, W-C Yang, K.A. Oglesby and K.D. Osborne, *The Development of Ford's P2000 Fuel Cell Vehicle*, SAE Paper 2000-01-1061.

S. Akella, N. Sivashankar and S. Gopalswamy, *Model-based systems analysis of a hybrid fuel cell vehicle configuration*, Proceedings of 2001 American Control Conference, 2001.

J.C. Amphlett, R.M. Baumert, R.F. Mann, B.A. Peppley, P.R. Roberge and A. Rodrigues, *Parametric modelling of the performance of a 5-kW proton-exchange membrane fuel cell stack*, Journal of Power Sources, v.49, pp. 349-356, 1994.

J.C. Amphlett, R.M. Baumert, R.F. Mann, B.A. Peppley and P.R. Roberge, *Performance modeling of the Ballard Mark IV solid polymer electrolyte fuel cell*, Journal of Electrochemical Society, v.142, n.1, pp.9-15, 1995.

P. Atwood, S. Gurski, D.J. Nelson, K.B. Wipke and T. Markel, *Degree of hybridiztion ADVISOR modeling of a fuel cell hybrid electric sport utility vehicle*, Proceedings of 2001 Joint ADVISOR/PSAT vehicle systems modeling user conference, pp.147-155, 2001.

F. Barbir, B. Balasubramanian and J. Neutzler, *Trade-off design analysis of operating pressure and temperature in PEM fuel cell systems*, Proceedings of the ASME Advanced Energy Systems Division, v.39, pp.305-315, 1999.

J.J. Baschuk and X. Li, *Modeling of polymer electrolyte membrane fuel cells with variable degreees of water flooding*, Journal of Power Sources, v.86, pp.186-191, 2000.

D.M. Bernardi and M.W. Verbrugge, *A Mathematical model of the solid-polymer-electrolyte fuel cell*, Journal of the Electrochemical Society, v.139, n.9, pp. 2477-2491, 1992.

D.D. Boettner, G. Paganelli, Y.G. Guezennec, G. Rizzoni and M.J. Moran, *Proton exchange membrane (PEM) fuel cell system model for automotive vehicle simulation and control*, Proceedings of 2001 ASME International Mechanical Engineering Congress and Exposition, 2001.

D.D. Boettner, G. Paganelli, Y.G. Guezennec, G. Rizzoni and M.J. Moran, *Component power sizing and limits of operation for proton exchange membrane (PEM) fuel cell/battery hybrid automotive applications*, Proceedings of 2001 ASME International Mechanical Engineering Congress and Exposition, 2001.

J.M. Cunningham, M.A Hoffman, R.M Moore and D.J. Friedman, *Requirements for a Flexible and Realistic Air Supply Model for Incorporation into a Fuel Cell Vehicle (FCV) System Simulation*, SAE Paper 1999-01-2912.

D.J. Friedman, A. Egghert, P. Badrinarayanan and J. Cunningham, *Balancing stack, air supply and water/thermal management demands for an indirect methanol PEM fuel cell system*, SAE Paper 2001-01-0535.

L. Guzzella, *Control Oriented Modelling of Fuel-Cell Based Vehicles*, Presentation in NSF Workshop on the Integration of Modeling and Control for Automotive Systems, 1999.

K-H Hauer, D.J. Friedmann, R.M. Moore, S. Ramaswamy, A. Eggert and P. Badrinarayana, *Dynamic Response of an Indirect-Methanol Fuel Cell Vehicle*, SAE Paper 2000-01-0370.

K. Kordesch and G. Simader, *Fuel Cells and Their Applications*, Weinheim, Germany, VCH, 1996.

J. Larminie and A. Dicks, *Fuel Cell Systems Explained*, West Sussex, England, John Wiley & Sons Inc, 2000.

F. Laurencelle, R. Chahine, J. Hamelin, K. Agbossou, M. Fournier, T.K. Bose and A. Laperriere, *Characterization of a Ballard MK5-E proton exchange membrane fuel cell stack*, Fuel Cells Journal, v.1, n.1, pp.66-71, 2001.

J.H. Lee, T.R. Lalk and A.J. Appleby, *Modeling electrochemical performance in large scale proton exchange membrane fuel cell stacks*, Journal of Power Sources, v.70, pp.258-268, 1998.

J.H. Lee and T.R. Lalk, *Modeling fuel cell stack systems*, Journal of Power Sources, v.73, pp.229-241, 1998.

P. Moraal and I. Kolmanovsky, *Turbocharger Modeling for Automotive Control Applications*, SAE Paper 1999-01-0908.

T.V. Nguyen and R.E. White, *A Water and Heat Management Model for Proton-Exchange-Membrane Fuel Cells*, Journal of Electrochemical Society, v.140, n.8, pp.2178-2186, 1993.

J. Padulles, G.W. Ault, C.A. Smith and J.R. McDonald, *Fuel cell plant dynamic modelling for power systems simulation*, Proceedings of 34th universities power engineering conference, v.34, n.1, pp.21-25, 1999.

S. Pischinger, C. Schönfelder, W. Bornscheuer, H. Kindl and A. Wiartalla, *Integrated Air Supply and Humidification Concepts for Fuel Cell Systems*, SAE Paper 2001-01-0233.

J.T. Pukrushpan, A.G. Stefanopoulou, H. Peng, *Modeling and Control for PEM Fuel Cell Stack System*, Proceedings of the American Control Conference, Anchorage, AK, pp.3117-3122, 2002.

T.E. Springer, T.A. Zawodzinski and S. Gottesfeld, *Polymer Electrolyte Fuel Cell Model*, Journal of Electrochemical Society, v.138, n.8, pp.2334-2342, 1991.

P. Thomas, *Simulation of Industrial Processes for Control Engineer*, London, Butterworth Heinemann, 1999.

W. Turner, M. Parten, D. Vines, J. Jones and T. Maxwell, *Modeling a PEM fuel cell for use in a hybrid electric vehicle*, Proceedings of the 1999 IEEE 49th Vehicular Technology Conference, v.2, pp.1385-1388, 1999.

W-C Yang and B. Bates and N. Fletcher and R. Pow, *Control Challenges and Methodologies in Fuel Cell Vehicle Development*, SAE Paper 98C054.

Appendix A: Useful Flow Calculations

In this section, we first explain the calculation of total mass flow rate between two volumes using nozzle equations. Then we explain the calculation of mass flow rates of each species (O_2, N_2 and vapor) in and out of the cathode channel air flow property. The flow rates are used in the mass balance equations (17)-(19).

The nozzle flow equation (Thomas, 1999) is used to calculate the flow between two volumes. The rate of flow pass through a nozzle is a function of upstream pressure, p_u, and downstream pressure, p_d, of the nozzle. The flow characteristic is divided into two regions by the critical pressure ratio:

$$pr_{crit} = \left(\frac{p_d}{p_u}\right)_{crit} = \left(\frac{2}{\gamma+1}\right)^{\frac{\gamma}{\gamma-1}} \tag{31}$$

where γ is the ratio of the specific heat capacities of the gas, C_p/C_v. For sub-critical (normal) flow where pressure drop is less than critical pressure ratio, $pr > pr_{crit}$, the mass flow rate is calculated from

$$W = \frac{C_D A_T p_u}{\sqrt{RT_1}} (pr)^{\frac{1}{\gamma}} \left\{ \frac{2\gamma}{\gamma-1} \left[1 - (pr)^{\frac{\gamma-1}{\gamma}} \right] \right\}^{\frac{1}{2}}. \tag{32}$$

The parameters C_D is the discharge coefficient of the nozzle, A_T is the opening area of the nozzle (m^2) and R is the universal gas constant. For critical (choked) flow, $pr \leq pr_{crit}$ the mass flow rate is given by

$$W_{choked} = \frac{C_D A_T p_1}{\sqrt{RT_1}} \gamma^{\frac{1}{2}} \left(\frac{2}{\gamma+1}\right)^{\frac{\gamma+1}{2(\gamma-1)}}. \tag{33}$$

If the pressure different across the nozzle is small, the flow rate can be calculated by the linearized form of the subcritical nozzle flow equation (32),

$$W = k_{nozzle}(p_u - p_d) \tag{34}$$

where k_{nozzle} is a constant.

Typically, air flow properties are given in terms of total mass flow rate, W, pressure, p, temperature, T, relative humidity (RH), ϕ, and dry air oxygen mole fraction, x_{O_2}. The total mass flow rate, W, is calculated based on upsteam and downsteam pressure using a linearized nozzle equation (34) for the cathode inlet flow. The humidity ratio is first used to separate the total flow rate into the flow rates of vapor and dry air. Then, the dry air flow rate is divided into oxygen and nitrogen flow rates using the definition of x_{O_2}.

Assuming ideal gases, the vapor pressure is calculated from the definition of the relative humidity

$$p_v = \phi p_{sat}(T) \tag{35}$$

where $p_{sat}(T)$ is vapor saturation pressure which is a function of gas temperature. Since humid air is a mixture of dry air and vapor, the dry air partial pressure is therefore the difference between total pressure and vapor pressure $p_a = p - p_v$. The humidity ratio, ω, defined as a ratio between mass of vapor and mass of dry air in the gas can be calculated as

$$\omega = \frac{M_v}{M_a}\frac{p_v}{p_a} \tag{36}$$

where M_v and M_a are vapor molar mass and inlet air molar mass, respectively. The molar mass of air, M_a, depends on the composition of the air and can be calculated from dry air oxygen mole fraction:

$$M_a = x_{O_2} \times M_{O_2} + (1 - x_{O_2}) \times M_{N_2} \tag{37}$$

where M_{O_2} and M_{N_2} are the molar mass of oxygen and nitrogen, respectively. The oxygen mole fraction, x_{O_2}, is 0.21 for inlet atmospheric air but varies for stack exit air. Based on the definition of the humidity ratio, the flow rate of dry air and and vapor are

$$W_a = \frac{1}{1+\omega}W \tag{38}$$

$$W_v = W - W_a \tag{39}$$

and the oxygen and nitrogen mass flow rate can be calculated by

$$W_{O_2} = y_{O_2} W_a \tag{40}$$

$$W_{N_2} = (1 - y_{O_2}) W_a \tag{41}$$

where, y_{O_2}, defined by $y_{O_2} = m_{O_2}/m_{dryair}$, is the oxygen mass fraction which is a function of dry air oxygen mole fraction, x_{O_2}.

$$y_{O_2} = \frac{x_{O_2} \times M_{O_2}}{x_{O_2} \times M_{O_2} + (1 - x_{O_2}) \times M_{N_2}} \tag{42}$$

Note again that x_{O_2} is constant for atmospheric air and varies for the stack outlet flow.

The calculation of hydrogen and vapor flow rates into the anode is similar to that of the air into the cathode, with the simplification that the anode gas contains pure hydrogen and vapor ($x_{H_2} = 1$). The calculation can also be applied to reformated hydrogen feed by modifying the hydrogen mole fraction in the reformed gas stream to the anode.